Tuning Mesophase of Ammonium Amphiphile-Encapsulated Polyoxometalate Complexes through Changing Component Structure

Wen Li, Shengyan Yin, Jinfeng Wang, and Lixin Wu*

State Key Laboratory of Supramolecular Structure and Materials, Jilin University, Changchun 130012, P. R. China

Received October 13, 2007. Revised Manuscript Received November 22, 2007

A series of biphenyl-containing ammonium amphiphiles with two alkyl chains, *N,N*-di[10-[4-(4′-alkyloxybiphenyl)oxy]decyl]-*N,N*-dimethylammonium bromide ($C_nBphC_{10}N$, $n = 6, 8, 10, 12$), were designed and synthesized to cap the polyoxometalates (PMs), forming corresponding amphiphile-encapsulated complexes (PM-m/$C_nBphC_{10}N$). To understand the effect of organic and inorganic components on the mesomorphic behavior of hybrid materials, we examined the thermal properties of these complexes and their organic components as the comparison using differential scanning calorimetry, polarized optical microscopy, and X-ray diffraction. The mesophase type of PM-1/$C_nBphC_{10}N$ is independent of the variety of tail length of amphiphiles. However, different smectic phases, such as smectic A, smectic C, smectic B, and crystalline smectic phases, can be obtained by appropriate selection of the polyoxometalates (PM-2, PM-3, and PM-4) with different shape and surface charge density. The present results provide a direct correlation between liquid crystalline properties of the hybrid complex and the feature of inorganic PMs.

Introduction

Multifunctional liquid crystals (LCs) have attracted much attention over recent years due to their potential applications in displays, sensors, smart materials, and so forth.[1] A typical example is metallomesogens, of which metal ions can be incorporated into organic LCs through precisely selected supramolecular interactions and present fluidity in mesophase.[2] The resulting hybrids allow the development of promising LCs with optical,[3] electronic,[4] and magnetic properties.[5] In spite of numerous studies, these functional LCs is mainly limited to the general complexes of metal ions. Comparing with simple metal ions, inorganic nanoparticles and clusters exhibit specific physical properties. Therefore, the fabrication of organic/inorganic nanohybrids combining the intrinsic properties of nanoparticles and/or clusters with organic LCs represents a new perspective in the area of multifunctional LCs. Additionally, it is expected that the hybrid LCs can promote the following synergistic property: (1) the grafting of particles or clusters can both introduce specific properties into LC system and provide the possibility to alter the dielectric behavior of organic LCs;[6] (2) the combination of LCs with particles or clusters will open up new scope for bottom-up self-organization of particles by controlling the type of mesophases.[7] Recently, gold, TiO_2, and Fe_2O_3 nanoparticles have been introduced successfully into LC systems,[8] whereas rare reports focus on LCs containing inorganic clusters,[9] in particular the polyoxometalates (PMs) clusters.

As a kind of attractive nanosized metal oxide clusters, PMs possess appealing electronic, optical, and magnetic properties, which exhibit diverse applications in chemistry and materials

* To whom correspondence should be addressed. E-mail: wulx@jlu.edu.cn.

(1) (a) Saez, I. M.; Goodby, J. W. *J. Mater. Chem.* **2005**, *15*, 26. (b) Kato, T.; Mizoshita, N.; Kishimoto, K. *Angew. Chem., Int. Ed.* **2006**, *45*, 38. (c) Tschierske, C. *Mater. Chem.* **2001**, *11*, 2647. (d) Gin, D. L.; Lu, X.; Nemade, P. R.; Pecinovsky, C. S.; Xu, Y.; Zhou, M. *Adv. Funct. Mater.* **2006**, *16*, 865.

(2) (a) Hudson, S. A.; Maitilis, P. M. *Chem. Rev.* **1993**, *93*, 861. (b) Binnemans, K.; Görller-Walrand, C. *Chem. Rev.* **2002**, *102*, 2303. (c) Piguet, C.; Bünzli, J. G.; Donnio, B.; Guillon, D. *Chem. Commun.* **2006**, *36*, 3755. (d) Serrano, J. L., Ed. *Metallomesogens: Synthesis and Applications*; VCH: Weinheim, 1996. (e) Donnio, B.; Guillon, D.; Deschenaux, R.; Bruce, D. W. In *Comprehensive Coordination Chemistry*; McCleverty, J. A., Meyer, T. J., Eds.; Elsevier: Oxford, 2003; Vol. 7, pp 357–627.

(3) (a) Bayon, R.; Coco, S.; Espinet, P. *Chem.—Eur. J.* **2005**, *11*, 1079. (b) SuFrez, S.; Imbert, D.; Gumy, F.; Piguet, C.; Bünzli, J.-C. G. *Chem. Mater.* **2004**, *16*, 3257. (c) Pucci, D.; Barberio, G.; Bellusci, A.; Crispini, A.; Donnio, B.; Giorgini, L.; Ghedini, M.; Deda, M. L.; Szerb, E. I. *Chem.—Eur. J.* **2006**, *12*, 6738. (d) Guillet, E.; Imbert, D.; Scopelliti, R.; Bünzli, J.-C. G. *Chem. Mater.* **2004**, *16*, 4063. (e) Damm, C.; Israel, G.; Hegmann, T.; Tschierske, C. *J. Mater. Chem.* **2006**, *16*, 1808.

(4) Matsuo, Y.; Muramatsu, A.; Kamikawa, Y.; Kato, T.; Nakamura, E. *J. Am. Chem. Soc.* **2006**, *128*, 9586.

(5) Barberá, J.; Giménez, R.; Marcos, M.; Serrano, J. L.; Alonso, P. J.; Martínez, J. I. *Chem. Mater.* **2003**, *15*, 958.

(6) (a) Reznikov, Y.; Buchnev, O.; Tereshchenko, O.; Reshetnyak, V.; Glushchenko, A.; West, J. *Appl. Phys. Lett.* **2003**, *82*, 1917. (b) Qi, H.; Hegmann, T. *J. Mater. Chem.* **2006**, *16*, 4197.

(7) (a) In, I.; Jun, Y.-K.; Kim, Y. J.; Kim, S. Y. *Chem. Commun.* **2005**, 800. (b) Yamada, M.; Shen, Z.; Miyake, M. *Chem. Commun.* **2006**, 2569. (c) Cseh, L.; Mehl, G. H. *J. Mater. Chem.* **2007**, *17*, 311.

(8) (a) Cseh, L.; Mehl, G. H. *J. Am. Chem. Soc.* **2006**, *128*, 13376. (b) Kanayama, N.; Tsutsumi, O.; Kanazawa, A.; Ikeda, T. *Chem. Commun.* **2001**, 2640. (c) Kanie, K.; Muramatsu, A. *J. Am. Chem. Soc.* **2005**, *127*, 11578. (d) Kanie, K.; Sugimoto, T. *J. Am. Chem. Soc.* **2003**, *125*, 10518.

(9) (a) Jiang, T.; Ozin, G. A. *J. Mater. Chem.* **1997**, *7*, 2213. (b) Camerel, F.; Antonietti, M.; Faul, C. F. J. *Chem.—Eur. J.* **2003**, *9*, 2160. (c) Riley, A. E.; Tolbert, S. H. *J. Am. Chem. Soc.* **2003**, *125*, 4551. (d) Zhang, T.; Spitz, C.; Antonietti, M.; Faul, C. F. J. *Chem.—Eur. J.* **2005**, *11*, 1001.

10.1021/cm702955j CCC: $40.75 © 2008 American Chemical Society
Published on Web 01/01/2008

Scheme 1. Synthetic Path for Biphenyl-Containing Amphiphiles

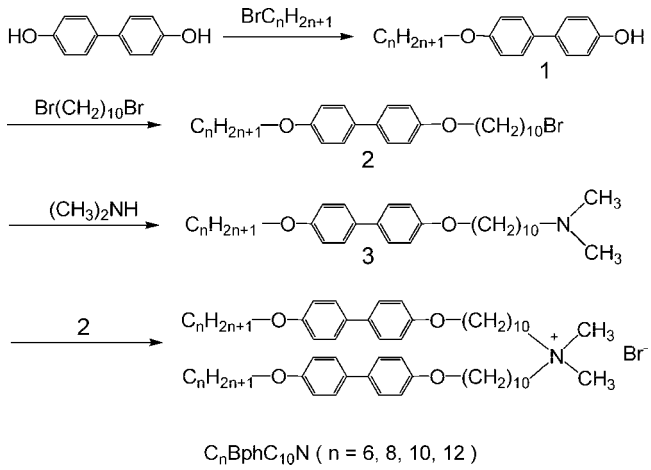

$C_nBphC_{10}N$ (n = 6, 8, 10, 12)

science.[10] Introduction of PMs into LCs would direct novel functional LCs. Several research groups have demonstrated that the coverage of anionic clusters with cationic surfactants could lead to ordered assembles, such as single monolayers,[11] LB films,[12] ordered microporous structures,[13] and vesicular assemblies.[14] Polarz and co-workers showed the first example about PM-based LCs using simple ammonium surfactant to encapsulate wheel-shaped PM.[15] In ordered to develop a general method to fabricate PM-containing LCs, we designed and synthesized a mesomorphic amphiphile, and the resulting amphiphile-encapsulated PMs complexes exhibited interesting thermotropic LC characteristics.[16a] We further investigated the conformational dynamics of the complexes.[16b] Now, it is necessary to deeply understand the relationship between the liquid crystalline properties and the structure of components because it is useful for controlling the self-organization process and the self-assembling ability of the complexes into periodically ordered meso- and nanostructures. In this report, we present a detailed investigation of the phase behavior of the complexes with variable tail length of amphiphiles and morphology of PMs. First, well-chosen biphenyl-containing cationic amphiphiles ($C_nBphC_{10}N$) with different tail lengths (Scheme 1) were synthesized, and their thermal properties were examined. Second, we encapsulated an elliptical hetero-polyoxotungatate cluster $K_{15}[Eu(BW_{11}O_{39})_2]\cdot 16H_2O$ (PM-1) (Figure 1) with $C_nBphC_{10}N$ to prepare the amphiphile-encapsulated complexes (PM-1/$C_nBphC_{10}N$). The influence of the tail length of amphiphiles on the thermal properties of PM-1/$C_nBphC_{10}N$ was systematically characterized by differential scanning calorimetry (DSC), polarized optical microscopy (POM), and X-ray diffraction (XRD). Third, we extended the clusters from elliptical cluster PM-1 to spherical clusters $K_5BW_{12}O_{40}\cdot 5H_2O$ (PM-2), $H_3PW_{12}O_{40}\cdot 8H_2O$ (PM-3), and a planar cluster $(NH_4)_3[ZnH_6Mo_6O_{24}]\cdot 10H_2O$ (PM-4) (Figure 1). $C_8BphC_{10}N$ was employed to encapsulate these clusters, and the as-prepared complexes PM-m/$C_8BphC_{10}N$ exhibit new and more interesting structures. This investigation proposes an interesting relationship between LC property and component structure.

Experimental Section

1. Preparation of Amphiphiles. 4,4′-Dihydroxybiphenyl was purchased from Aldrich, and 1,10-dibromodecane was obtained from Fluka and used without further purification. Other starting compounds and solvents applied in the preparation were commercial products from local chemical reagent company. Doubly distilled water was used in the experiments. Silica gel (100–200 mesh) was employed for the purification of column chromatography. The synthesis of amphiphiles ($C_nBphC_{10}N$) was carried out following the modified routes of the literature,[17–19] as shown in Scheme 1. Detailed procedures for one of them, *N*,*N*-di[10-[4-(4′-hexyloxybiphenyl)oxy]decyl]-*N*,*N*-dimethylammonium bromide ($C_6BphC_{10}N$), are as follows.

*4-Hydroxyl-4′-hexyloxybiphenyl (***1***).* A mixture of 4,4′-dihydroxybiphenyl (6 g, 33 mmol), 1-bromohexane (4.95 g, 30 mmol), and anhydrous K_2CO_3 (5 g, 36 mmol) was stirred for 24 h under refluxing. After being poured into water, the mixture was acidified with diluted HCl solution. The solid product was collected and purified through column chromatography on silica gel using $CHCl_3$ as eluent. Yield: 44%.

*4-(10-Bromodecyloxy)-4′-hexyloxybiphenyl (***2***).* A mixture of **1** (3.62 g, 13.4 mmol), 1,10-dibromodecane (4.82 g, 16.06 mmol), and anhydrous K_2CO_3 (2.82 g, 20 mmol) in 120 mL of acetone was stirred for 24 h under refluxing. The solvent was evaporated, and the residue was treated with chloroform and filtered. The organic phase was washed with water, dried over anhydrous $MgSO_4$, and filtered. After evaporating solvent, the residue was further purified to give **2** through column chromatography on silica gel using chloroform/petroleum ether (3:1, v/v) as eluent. Yield: 60%.

*N-[10-[4-(4′-Hexyloxybiphenyl)oxy]decyl]-N,N-dimethylamine (***3***).* A mixture of **2** (0.95 g, 1.93 mmol) and 33% dimethylamine aqueous solution (2.4 g, 9.65 mmol) in 35 mL of ethanol was stirred for 24 h under refluxing. The solvent was evaporated under reduced pressure, the residue was treated with chloroform, and the organic phase was washed with water, dried over anhydrous $MgSO_4$, and filtered. After the evaporation of solvent, the residue was purified to obtain **3** through column chromatography on silica gel using $CHCl_3/CH_3OH$ (12/1, v/v) as eluent. Yield: 84%. ^1H NMR ($CDCl_3$, 500 MHz): $\delta = 0.89$ (t, $J = 7$ Hz, 3 H), $\delta = 1.26$–1.31 (m, 16 H), $\delta = 1.44$–1.48 (m, 4 H), $\delta = 1.77$–1.82 (m, 4 H), $\delta = 2.44$ (s, 6 H), $\delta = 2.53$ (t, $J = 10$ Hz, 2 H), $\delta = 4.00$ (t, $J = 5$ Hz, 4 H), $\delta = 6.93$–6.95 (d, $J = 10$ Hz, 4 H), $\delta = 7.44$–7.46 (d, $J = 10$ Hz, 4 H).

(10) (a) Pope, M. T.; Müller, A. *Angew. Chem., Int. Ed.* **1991**, *30*, 34. (b) Hill, C. L.; Prosser-McCartha, C. M. *Coord. Chem. Rev.* **1995**, *143*, 407. (c) Hill, C. L. *Chem. Rev.* **1998**, *98* (the entire issue).
(11) (a) Kurth, D. G.; Lehmann, P.; Volkmer, D.; Cölfen, H.; Koop, M. J.; Müller, A.; Du Chesne, A. *Chem.—Eur. J.* **2000**, *6*, 385. (b) Volkmer, D.; Du Chesne, A.; Kurth, D. G.; Schnablegger, H.; Lehmann, P.; Koop, M. J.; Müller, A. *J. Am. Chem. Soc.* **2000**, *122*, 1995. (c) Bu, W.; Fan, H.; Wu, L.; Hou, X.; Hu, C.; Zhang, G.; Zhang, X. *Langmuir* **2002**, *18*, 6398.
(12) (a) Kurth, D. G.; Lehmann, P.; Volkmer, D.; Müller, A.; Schwahn, D. *J. Chem. Soc., Dalton Trans.* **2000**, 3989. (b) Bu, W.; Li, H.; Li, W.; Wu, L.; Zhai, C.; Wu, Y. *J. Phys. Chem. B* **2004**, *108*, 12776.
(13) (a) Bu, W.; Li, H.; Sun, H.; Yin, S.; Wu, L. *J. Am. Chem. Soc.* **2005**, *127*, 8016. (b) Sun, H.; Li, H.; Bu, W.; Xu, M.; Wu, L. *J. Phys. Chem. B* **2006**, *110*, 24847.
(14) Li, H.; Sun, H.; Qi, W.; Xu, M.; Wu, L. *Angew. Chem., Int. Ed.* **2007**, *46*, 1300.
(15) Polarz, S.; Smarsly, B.; Antonietti, M. *ChemPhysChem* **2001**, *2*, 457.
(16) (a) Li, W.; Bu, W.; Li, H.; Wu, L.; Li, M. *Chem. Commun.* **2005**, 3785. (b) Li, W.; Yin, S.; Wu, Y.; Wu, L. *J. Phys. Chem. B* **2006**, *110*, 16961.
(17) Ohtake, T.; Ogasawara, M.; Ito-Akita, K.; Nishina, N.; Ujiie, S.; Ohno, H.; Kato, T. *Chem. Mater.* **2000**, *12*, 782.
(18) Okahata, Y.; Ando, R.; Kunitake, T. *Bull. Chem. Soc. Jpn.* **1979**, *52*, 3647.
(19) Ueoka, R.; Matsumoto, Y. *J. Org. Chem.* **1984**, *49*, 3774.

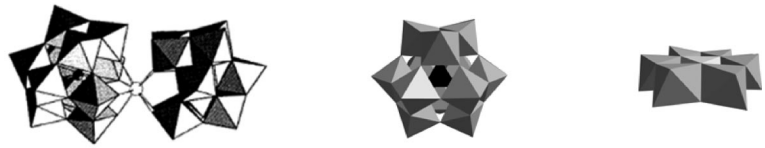

PM-1 $K_{15}[Eu(BW_{11}O_{39})_2]$ PM-2: $K_5BW_{12}O_{40}$ PM-3: $H_3PW_{12}O_{40}$ PM-4 $(NH_4)_3[ZnH_6Mo_6O_{24}]$

Figure 1. Structure representation of $K_{15}Eu(BW_{11}O_{39})_2$ (PM-1), $K_5BW_{12}O_{40}$ (PM-2), $H_3PW_{12}O_{40}$ (PM-3), and $(NH_4)_3[ZnH_6Mo_6O_{24}]$ (PM-4).

N,N-Di[10-[4-(4′-hexyloxybiphenyl)oxy]decyl]-N,N-dimethylammonium Bromide ($C_6BphC_{10}N$). A mixture of **3** (0.47 g, 1 mmol), **2** (0.59 g, 1.2 mmol), and anhydrous Na_2CO_3 (1.0 g, 9.4 mmol) in 80 mL of ethanol was refluxed for 24 h. The solvent was evaporated, the resulting reaction mixture was treated with chloroform, and the undissolved salt was removed by filtration. The filtrate was washed with water, dried over anhydrous $MgSO_4$, and then concentrated under reduced pressure. The residue was purified to give the final product through column chromatography on silica gel using $CHCl_3$/CH_3OH (10/1, v/v) as eluent Yield: 80%. ^1H NMR ($CDCl_3$, 500 MHz): $\delta = 0.91$ (t, $J = 7$ Hz, 6 H), $\delta = 1.29$–1.35 (m, 32 H), $\delta = 1.44$–1.48 (m, 8 H), $\delta = 1.78$–1.81 (m, 8 H), $\delta = 3.36$ (s, 6 H), $\delta = 3.50$ (t, $J = 10$ Hz, 4 H), $\delta = 3.98$ (t, $J = 6$ Hz, 8 H), $\delta = 6.92$–6.94 (d, $J = 10$ Hz, 8 H), $\delta = 7.44$–7.46 (d, $J = 10$ Hz, 8 H). IR (KBr, cm^{-1}): $\nu = 3446$, 2956, 2922, 2870, 2852, 1606, 1501, 1473, 1467, 1396, 1272, 1247, 1178, 1037, 995, 822, 808, 725, 595, 516. Anal. Calcd for amphiphile $C_6BphC_{10}N$ (979.26): C, 71.14; H, 9.47; N, 1.43. Found: C, 71.21; H, 9.27; N, 1.31. Corresponding formula: $C_{58}H_{88}NO_4Br\cdot 2H_2O$.

N,N-Di[10-[4-(4′-octyloxybiphenyl)oxy]decyl]-N,N-dimethylammonium Bromide ($C_8BphC_{10}N$). Compound $C_8BphC_{10}N$ was synthesized similarly to $C_6BphC_{10}N$, by using 1-bromooctane instead of 1-bromohexane. ^1H NMR ($CDCl_3$, 500 MHz): $\delta = 0.89$ (t, $J = 7$ Hz, 6 H), $\delta = 1.29$–1.37 (m, 40 H), $\delta = 1.44$–1.48 (m, 8 H), $\delta = 1.78$–1.81 (m, 8 H), $\delta = 3.36$ (s, 6 H), $\delta = 3.50$ (t, $J = 10$ Hz, 4 H), $\delta = 3.98$ (t, $J = 6$ Hz, 8 H), $\delta = 6.93$–6.95 (d, $J = 10$ Hz, 8 H), $\delta = 7.44$–7.46 (d, $J = 10$ Hz, 8 H). Anal. Calcd for amphiphile $C_8BphC_{10}N$ (1017.35): C, 73.20; H, 9.71; N, 1.38. Found: C, 72.71; H, 9.67; N, 1.11. Corresponding formula: $C_{62}H_{96}NO_4Br\cdot H_2O$.

N,N-Di[10-[4-(4′-decyloxybiphenyl)oxy]decyl]-N,N-dimethylammonium Bromide ($C_{10}BphC_{10}N$). Compound $C_{10}BphC_{10}N$ was obtained similarly to $C_6BphC_{10}N$, by using 1-bromodecane instead of 1-bromohexane. ^1H NMR ($CDCl_3$, 500 MHz): $\delta = 0.88$ (t, $J = 7$ Hz, 6 H), $\delta = 1.28$–1.37 (m, 48 H), $\delta = 1.43$–1.48 (m, 8 H), $\delta = 1.78$–1.80 (m, 8 H), $\delta = 3.36$ (s, 6 H), $\delta = 3.50$ (t, $J = 10$ Hz, 4 H), $\delta = 3.98$ (t, $J = 6$ Hz, 8 H), $\delta = 6.92$–6.94 (d, $J = 10$ Hz, 8 H), $\delta = 7.44$–7.46 (d, $J = 10$ Hz, 8 H). Anal. Calcd for amphiphile $C_{10}BphC_{10}N$ (1073.46): C, 75.10; H, 9.93; N, 1.32. Found: C, 74.89; H, 9.68; N, 1.24. Corresponding formula: $C_{66}H_{104}NO_4Br\cdot H_2O$.

N,N-Di[10-[4-(4′-dodecyloxybiphenyl)oxy]decyl]-N,N-dimethylammonium Bromide ($C_{12}BphC_{10}N$). Compound $C_{12}BphC_{10}N$ was obtained similarly to $C_6BphC_{10}N$, by using 1-bromododecane instead of 1-bromohexane. ^1H NMR ($CDCl_3$, 500 MHz): $\delta = 0.88$ (t, $J = 7$ Hz, 6 H), $\delta = 1.29$–1.37 (m, 56 H), $\delta = 1.44$–1.48 (m, 8 H), $\delta = 1.78$–1.81 (m, 8 H), $\delta = 3.36$ (s, 6 H), $\delta = 3.50$ (t, $J = 10$ Hz, 4 H), $\delta = 3.98$ (t, $J = 6$ Hz, 8 H), $\delta = 6.93$–6.95 (d, $J = 10$ Hz, 8 H), $\delta = 7.44$–7.46 (d, $J = 10$ Hz, 8 H). Anal. Calcd for amphiphile $C_{12}BphC_{10}N$ (1147.58): C, 75.64; H, 10.16; N, 1.26. Found: C, 75.32; H, 9.97; N, 1.13. Corresponding formula: $C_{70}H_{112}NO_4Br\cdot 2H_2O$.

2. General Procedure for Preparation of LC Complexes. Metal oxide clusters PM-1,[20] PM-2,[21] and PM-4[22] were freshly prepared according to the procedures as described in the literature. PM-3 was directly obtained from Fluka.

PM-1/$C_6BphC_{10}N$. It was synthesized using the procedures of the literature.[16] PM-1 was dissolved in aqueous solution (pH = 5.7), and then $C_6BphC_{10}N$ in chloroform solution was added. The mixture was stirred for 4 h at 45 °C. The initial molar ratio of $C_6BphC_{10}N$ to PM-1 was controlled at 12:1. The organic phase was separated, and the complex was obtained by evaporating chloroform to dryness. Then, the sample was further dried in vacuum until the weight remained constant. IR (KBr, cm^{-1}): $\nu = 3452$, 2956, 2921, 2870, 2852, 1605, 1501, 1473, 1465, 1394, 1272, 1249, 1176, 1035, 997, 943, 898, 823, 810, 784, 726, 595, 516. Anal. Calcd for PM-1/$C_6BphC_{10}N$ ($C_{754}H_{1172}N_{13}O_{143}W_{22}B_2Eu$, 16925.44): C, 53.51; H, 6.98; N, 1.08. Found: C, 53.77; H, 7.16; N, 0.98. Thermogravimetric analysis (TGA) suggests a mass loss of 2.71% from 30 to 120 °C, arising from crystal water in PM-1/$C_6BphC_{10}N$. Combining TGA and elemental analysis, PM-1/$C_6BphC_{10}N$ should correspond to a tentative formula: $(C_6BphC_{10}N)_{13}H_2[Eu(BW_{11}O_{39})_2]\cdot 13H_2O$.

PM-1/$C_8BphC_{10}N$. It was synthesized following a similar procedure as for PM-1/$C_6BphC_{10}N$, by using $C_8BphC_{10}N$ instead. The initial molar ratio of $C_8BphC_{10}N$ to PM-1 was kept at 12:1. IR (KBr, cm^{-1}) for PM-1/$C_8BphC_{10}N$: $\nu = 3440$, 2956, 2921, 2871, 2852, 1606, 1500, 1473, 1465, 1396, 1272, 1247, 1178, 1035, 995, 945, 898, 823, 808, 781, 723, 595, 516. Anal. Calcd for PM-1/$C_8BphC_{10}N$ ($C_{806}H_{1304}N_{13}O_{157}W_{22}B_2Eu$, 17907.04): C, 54.06; H, 7.34; N, 1.02. Found: C, 53.77; H, 7.46; N, 0.88. Thermogravimetric analysis (TGA) suggests a mass loss of 2.68% from 30 to 130 °C, arising from crystal water in the complex. Combining TGA and elemental analysis, PM-1/$C_8BphC_{10}N$ should correspond to a formula: $(C_8BphC_{10}N)_{13}H_2[Eu(BW_{11}O_{39})_2]\cdot 27H_2O$.

PM-1/$C_{10}BphC_{10}N$. It was synthesized following a similar procedure as for PM-1/$C_6BphC_{10}N$, by using $C_{10}BphC_{10}N$ instead. The initial molar ratio of $C_{10}BphC_{10}N$ to PM-1 was controlled at 12:1. IR (KBr, cm^{-1}) for PM-1/$C_{10}BphC_{10}N$: $\nu = 3442$, 2954, 2921, 2871, 2852, 1606, 1500, 1473, 1465, 1396, 1272, 1247, 1178, 1035, 995, 948, 900, 823, 808, 781, 721, 595, 516. Anal. Calcd for PM-1/$C_{10}BphC_{10}N$ ($C_{858}H_{1384}N_{13}O_{145}W_{22}B_2Eu$, 18420.24): C, 55.94; H, 7.57; N, 0.99. Found: C, 55.69; H, 7.81; N, 0.90. Thermogravimetric analysis (TGA) suggests a mass loss of 1.46% from 30 to 120 °C arising from crystal water in PM-1/$C_{10}BphC_{10}N$. Combining TGA and elemental analysis, PM-1/$C_{10}BphC_{10}N$ should correspond to a formula: $(C_{10}BphC_{10}N)_{13}H_2[Eu(BW_{11}O_{39})_2]\cdot 15H_2O$.

PM-1/$C_{12}BphC_{10}N$. It was synthesized following a similar procedure as for PM-1/$C_6BphC_{10}N$, using $C_{12}BphC_{10}N$ instead. The initial molar ratio of $C_{12}BphC_{10}N$ to PM-1 was controlled at 12:1. IR (KBr, cm^{-1}) PM-1/$C_{12}BphC_{10}N$: $\nu = 3446$, 2954, 2919, 2871,

(20) Peacock, R. D.; Weakley, T. J. R. *J. Chem. Soc. A* **1971**, 1836.
(21) Weinstock, I. A.; Cowan, J. J.; Barbuzzi, E. M. G.; Zeng, H.; Hill, C. L. *J. Am. Chem. Soc.* **1999**, *121*, 4608.
(22) Nomiya, K.; Takahashi, T.; Shirai, T.; Miwa, M. *Polyhedron* **1987**, *6*, 213.

2850, 1606, 1500, 1473, 1467, 1394, 1272, 1247, 1178, 1037, 997, 943, 898, 823, 808, 781, 725, 597, 516. Anal. Calcd for PM-1/$C_{12}BphC_{10}N$ ($C_{910}H_{1508}N_{13}O_{155}W_{22}B_2Eu$, 19329.77): C, 56.54; H, 7.86; N, 0.94. Found: C, 56.65; H, 8.05; N, 0.85. Thermogravimetric analysis (TGA) suggests a mass loss of 2.3% from 30 to 150 °C arising from crystal water in PM-1/$C_{12}BphC_{10}N$. Combining TGA and elemental analysis, PM-1/$C_{12}BphC_{10}N$ should correspond to a formula: $(C_{12}BphC_{10}N)_{13}H_2[Eu(BW_{11}O_{39})_2]\cdot 25H_2O$.

PM-2/$C_8BphC_{10}N$. The initial molar ratio of $C_8BphC_{10}N$ to PM-2 was controlled at 5:1. Anal. Calcd for PM-2/$C_8BphC_{10}N$ ($C_{310}H_{496}N_5O_{68}W_{12}B$, 7598.14): C, 49.00; H, 6.58; N, 0.92. Found: C, 48.87; H, 6.49; N, 0. 89. Thermogravimetric analysis (TGA) suggests a mass loss of 1.89% from 30 to 110 °C arising from crystal water in PM-2/$C_8BphC_{10}N$. Combining TGA and elemental analysis, PM-2/$C_8BphC_{10}N$ should correspond to a tentative formula: $(C_8BphC_{10}N)_5(BW_{12}O_{40})\cdot 8H_2O$.

PM-3/$C_8BphC_{10}N$. The initial molar ratio of $C_8BphC_{10}N$ to PM-3 was controlled at 4:1. Anal. Calcd for PM-3/$C_8BphC_{10}N$ ($C_{186}H_{310}N_3O_{63}W_{12}P$, 5833.49): C, 38.30; H, 5.36; N, 0.72. Found: C, 38.13; H, 5.21; N, 0.68. Thermogravimetric analysis (TGA) suggests a mass loss of 3.99% from 30 to 100 °C arising from crystal water in PM-3/$C_8BphC_{10}N$. Combining the TGA and elemental analysis, PM-3/$C_8BphC_{10}N$ should correspond to a tentative formula: $(C_8BphC_{10}N)_3(PW_{12}O_{40})\cdot 11H_2O$.

PM-4/$C_8BphC_{10}N$. The initial molar ratio of $C_8BphC_{10}N$ to PM-4 was controlled at 3:1. Anal. Calcd for PM-4/$C_8BphC_{10}N$ ($C_{186}H_{316}N_3O_{47}Mo_6Zn$, 3987.52): C, 56.02; H, 7.99; N, 1.05. Found: C, 55.87; H, 7.62; N, 0.98. Thermogravimetric analysis (TGA) suggests a mass loss of 4.9% from 30 to 110 °C arising from crystal water in PM-4/$C_8BphC_{10}N$. Combining the TGA and elemental analysis, PM-4/$C_8BphC_{10}N$ should correspond to a tentative formula: $(C_8BphC_{10}N)_3[ZnH_6Mo_6O_{24}]\cdot 11H_2O$.

3. Specimen Preparation for TEM. The sample of complex PM-2/$C_8BphC_{10}N$ was heated on a heating stage over its highest endothermic transition temperature, holding the state isothermally for 2 min and then quenching to preset annealing temperature for 1 h. The annealing temperature was carefully selected to form high-ordered morphology where specific LC phase was formed. Then, the thin films were removed from the glass slide, floated on the water surface, and recovered using copper grids for transmission electron microscopy (TEM) observations.

4. Measurements. ^{1}H NMR spectra were recorded on a Bruker Avance 500 instrument using $CDCl_3$ as solvent and TMS as internal reference (0.00 ppm). Elemental analysis (C, H, N) was performed on a Flash EA1112 from ThermoQuest Italia SPA. FT-IR spectra were carried out on a Bruker IFS66V equipped with a DGTS detector with a resolution of 4 cm^{-1} from pressed KBr pellets. Thermogravimetric analysis (TGA) was conducted with a Perkin-Elmer TG/DTA-7 instrument, and the heating rate was set at 10 °C min^{-1}. The phase behaviors were measured using a polarized optical microscope (Leica DMLP, Germany) equipped with a Mettler FP82HT hot stage and a Mettler FP90 central processor. DSC measurements were performed on a Netzsch DSC 204 with scanning rate of 10 °C min^{-1}. The samples were sealed in aluminum capsules in air, and the atmosphere of holder was sustained under dry nitrogen. For variable-temperature XRD experiments, a Rigaku X-ray diffractometer (D/max 2500V, using Cu Kα_1 radiation of a wavelength of 0.154 nm) with a PTC-20A temperature controller was used. TEM experiments were carried out in JEOL-2010 electron microscope operating at 200 kV.

Results and Discussion

Preparation of Amphiphiles and Complexes. We synthesized four biphenyl-containing ammonium amphiphiles in which their tails were in variable lengths (see Scheme 1). The synthetic procedures were described in detail in the Experimental Section. In order to examine the influence of tail length of amphiphiles on thermal properties of complexes, we employed amphiphile $C_6BphC_{10}N$, $C_8BphC_{10}N$, $C_{10}BphC_{10}N$, and $C_{12}BphC_{10}N$ to encapsulate the elliptical cluster PM-1. The as-prepared complexes correspond to PM-1/$C_6BphC_{10}N$, PM-1/$C_8BphC_{10}N$, PM-1/$C_{10}BphC_{10}N$, and PM-1/$C_{12}BphC_{10}N$, respectively, and the thermal properties of all these complexes were characterized by DSC, POM, and XRD. In addition, $C_8BphC_{10}N$ was used to encapsulate spherical PM-2, PM-3, and planar PM-4, and the resulting complexes were PM-2/$C_8BphC_{10}N$, PM-3/$C_8BphC_{10}N$, and PM-4/$C_8BphC_{10}N$, respectively. The influence of the nature of PMs on phase behaviors of complexes was investigated by comparing their thermal properties of PM-1/$C_8BphC_{10}N$, PM-2/$C_8BphC_{10}N$, PM-3/$C_8BphC_{10}N$, and PM-4/$C_8BphC_{10}N$.

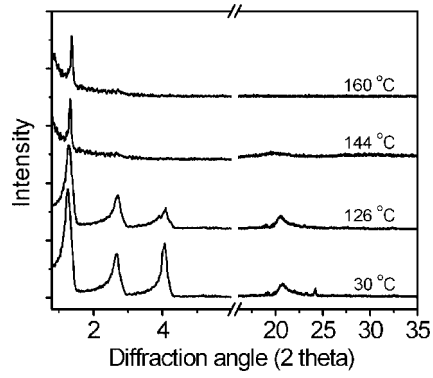

Figure 2. Temperature-dependent X-ray diffraction pattern of $C_{12}BphC_{10}N$.

Thermal Property of Biphenyl-Containing Amphiphiles $C_nBphC_{10}N$. The LC behaviors of amphiphiles, $C_nBphC_{10}N$, were investigated by DSC, POM, and XRD. DSC curves shown in Figure S1 (Supporting Information) illustrate phase transitions of $C_nBphC_{10}N$ in their second heating and cooling processes. The amphiphiles show a solid–solid transition. Practically, similar solid–solid phase transition was observed in the case of some amphiphilic molecules.[23] Figure S2 shows typical optical textures of smectic phases. Table S1 summarizes the phase transition temperatures, enthalpies, and assignments for all these amphiphiles. The identification of mesophases of $C_nBphC_{10}N$ has been further confirmed by XRD.

The XRD patterns of $C_{12}BphC_{10}N$ as a representative example are shown in Figure 2. A sharp diffraction in the small-angle region with a diffuse diffraction in the wide-angle region appears at 160 °C, suggesting a disordered smectic mesophase. Combining the optical texture and XRD data, we conclude that $C_{12}BphC_{10}N$ forms a smectic A phase, and the layer spacing is found to be 6.4 nm. This value is larger than the calculated single molecular length (L_s = 3.85 nm) but smaller than double the length, indicating the smectic

(23) (a) Busico, V.; Cernicchlaro, P.; Corradini, P.; Vacatello, M. *J. Phys. Chem.* **1983**, *87*, 1631. (b) Bowlas, C. J.; Bruce, D. W.; Seddon, K. R. *Chem. Commun.* **1996**, 1625. (c) Sudhölter, E. J. R.; Engberts, J. B. F. N.; de Jeu, W. H. *J. Phys. Chem.* **1982**, *86*, 1908. (d) Ubbelohde, A. R.; Michels, H. J.; Duruz, J. J. *Nature (London)* **1970**, *228*, 50.

Table 1. Summary of Assignments of Mesophases, Phase Transition Temperatures (°C), and Enthalpies (kJ/mol) of All the Complexes

		second cooling		second heating	
complexes	transition[a]	T (°C)	ΔH (kJ/mol)	T (°C)	ΔH (kJ/mol)
PM-1/$C_6BphC_{10}N$	S1−S2	101	17.2	105	20.2
	S2−SmC	131	33.9	132	36.9
	SmC−SmA	182	17.3	186	20.7
	SmA−Iso	215	31.1	215	33.1
PM-1/$C_8BphC_{10}N$	S1−S2	66	6.9		
	S2−SmC	119	238.7	122	245.1
	SmC−SmA	184	14.8	186	17.6
	SmA−Iso	216	26.2	217	28.5
PM-1/$C_{10}BphC_{10}N$	S1−S2	78	9.1	100	
	S2−SmC	112	363.2	114	386.2
	SmC−SmA	182	13.3	186	15.9
	SmA−Iso	217	20.4	218	18.3
PM-1/$C_{12}BphC_{10}N$	S1−S2	74	8.6		
	S2−SmC	106	422.1	109	432.3
	SmC−SmA	182	16.4	184	16.6
	SmA−Iso	217	19.3	217	28.3
PM-2/$C_8BphC_{10}N$	S1−S2	110		119	
	S2−SmC	130	42.6	134	45.5
	SmC−X[b]	182	11.5	185	12.1
	X−SmA	196	3.9	197	4.25
	SmA−Iso	223	21.3	225	21.2
PM-3/$C_8BphC_{10}N$	S1−S2	128	9.3	129	9.16
	S2−SmX[c]	191	25.8	194	26.2
	SmX−SmB	208	7.7	211	7.89
	SmB−Iso	247	21.5	255	27.9
PM-4/$C_8BphC_{10}N$	S−SmC	131	21.0	134	26.3
	SmC−SmA	159	2.3	162	3.82
	SmA−Iso	190	2.3	196	3.98

[a] S, SmC, SmB, SmA, and Iso indicate solid, smectic C, smectic B, smectic A, and isotropic phases, respectively. [b] X = unknown mesophase. [c] SmX = crystalline smectic phase.

A phase is a partially interdigated bilayer. When the temperature decreases to 145 °C, another smectic phase with an increased layer thickness of 6.7 nm forms, and the diffuse peak in the wide-angle region still exists. Considering the schlieren texture at this temperature, this mesophase can be ascribed to smectic C phase. When the temperature falls down to 126 °C, a crystalline smectic phase (smectic X) forms, where the layer distance is estimated to be 6.8 nm. All these amphiphiles can form layered structures, and the layer spacing values are listed in Table S2. It is well-known that the quaternary ammonium amphiphiles show smectic-like character,[24] but few of them show three different smectic phases. We think that the elongation of the tail length generates a variety of competitive interactions, which lead to different mesomorphic states. This result suggests that different smectic mesophases can be modulated by tuning the tail length of amphiphiles.

Influence of Tail Alkyl Chain Length on LC Behavior of Complexes. To understand the LC behavior dependence of the complexes on the tail length of amphiphile, we investigate the thermal property of a series of PM-1/$C_nBphC_{10}N$. Table 1 summarizes the phase transition temperatures, enthalpies, and assignments of all the complexes. Much higher enthalpy values can be observed for the transition S2−SmC of complexes, PM-1/$C_nBphC_{10}N$. In fact, from the Experimental Section, we can see that there are 13 ammonium amphiphiles in one complex. We come to a conclusion that the high enthalpies resulted from the summary of 13 amphiphiles per molar complex. In addition, we observed that the enthalpy values for the transition S2−SmC of complexes PM-1/$C_nBphC_{10}N$ decreased obviously with decreasing the length of tail alkyl chains of ammonium amphiphiles, which means that the enthalpy is related to the hydrophobic interaction among terminal alkyl chains.

When the elliptical PM-1 is encapsulated by $C_nBphC_{10}N$, the thermal properties of the resulting complexes PM-1/$C_nBphC_{10}N$ change significantly. As shown in the DSC traces of Figure 3, the transition temperature from solid to LC phase decreases gradually with increasing the tail length, which is similar to that of ammonium amphiphiles. Another remarkable feature is that the transition temperatures of PM-1/$C_nBphC_{10}N$ are identical in higher temperature region, and the transition does not occur under a sudden temperature change but rather a broad band. The result is consistent with our earlier observations, and we have presented[16] that the transition temperature of the complexes in the low-temperature region is associated with the hydrophobic interaction of the amphiphiles, whereas the temperature in the high-temperature region is related to the nature of PMs. The same inorganic core in the complexes PM-1/$C_nBphC_{10}N$ results in the same transition temperatures in high temperature region. Additionally, the broad peak in the high-temperature region is a result of the strong electrostatic interactions between the ammonium head groups and the PM.[16b]

As a representative sample, the polarizing optical micrographs of PM-1/$C_8BphC_{10}N$ are shown in Figure 4. Typical batonnet texture in the high-temperature LC region (Figure

(24) (a) Bowlas; C, J.; Bruce, D. W.; Seddon, K. R. *Chem. Commun.* **1996**, 1625. (b) Sudhölter, E. J. R.; Engberts, J. B. F. N.; de Jeu, W. H. *J. Phys. Chem.* **1982**, *86*, 1908. (c) Binnemans, K. *Chem. Rev.* **2005**, *105*, 4148.

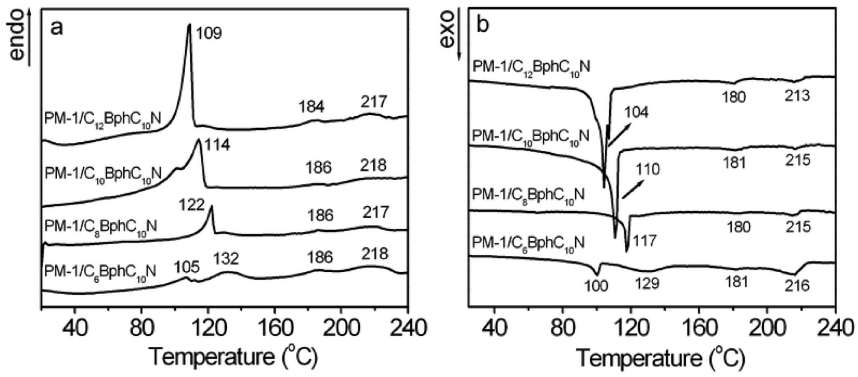

Figure 3. DSC curves of PM-1/C_nBphC_{10}N on their (a) second heating and (b) second cooling process.

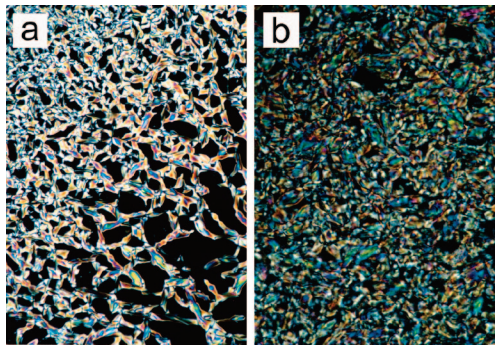

Figure 4. Polarizing optical micrographs of PM-1/C_8BphC_{10}N (a) at 204 °C and (b) at 170 °C (magnification: ×200).

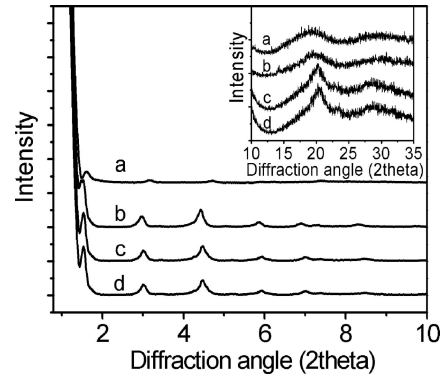

Figure 5. X-ray diffraction patterns of PM-1/C_8BphC_{10}N at (a) 210, (b) 160, (c) 110, and (d) 30 °C (inset: corresponding wide-angle X-ray diffractions).

4a) can be attributed to the smectic phase. During further cooling, broken texture appears in the low-temperature LC region (Figure 4b), suggesting another smectic phase. Similar optical images can also be observed for PM-1/C_6BphC_{10}N, PM-1/C_{10}BphC_{10}N, and PM-1/C_{12}BphC_{10}N (Figure S3). We have proposed that the thermal properties of complexes are quite similar to that of LC polymers, taking account of their molecular weights.[16] In fact, the batonnet texture is commonly found in LC polymers.[25] On the basis of optical textures, the phase in the high-temperature LC region is ascribed to smectic A phase and that in the low-temperature LC region is ascribed to smectic C phase for PM-1/C_8BphC_{10}N. These identifications can be supported by XRD data described below.

Figure 5 shows the XRD patterns of PM-1/C_8BphC_{10}N at variable temperatures. In the small-angle region, equidistant diffractions are found in all temperature ranges. It is also noted that the (003) reflection is higher than the (002) reflection, suggesting the complex has symmetrical double-layered structures. In the high-temperature LC region, the sample features a smectic A phase possessing a periodicity of 5.5 nm, as proved by the presence of a broad halo centered at $2\theta \approx 20°$ (Figure 5a, inset). We have presented[16,26] that most of amphiphile molecules align along the long axis of the elliptical cluster, which is favorable for the ordered and oriented packing in the lamellar structure. The short-axis diameter ($L_{PM\text{-}1}$) of PM-1 is 1 nm,[26,27] and the ideal molecular lengths (Ls) of C_nBphC_{10}N have been calculated to be 3.1, 3.4, 3.6, and 3.9 nm when n is 6, 8, 10, and 12, respectively. From Table S3, we can conclude that the layer spacing values (d) of PM-1/C_nBphC_{10}N in smectic A phase is $(L_s + L_{PM\text{-}1}) < d < (2L_s + L_{PM\text{-}1})$, indicating that the layered structure is composed of a PM-1 layer separated by interdigitated amphiphile bilayer. With cooling the temperature, smectic C phase should generate because of a diffuse peak appearing in the wide-angle region (Figure 5b), and the layer thickness is found to increase slightly ($d = 5.81$ nm). It is notable that the layer spacing values increase with decreasing temperature, and such a trend is similar to some ionic liquid crystals.[16,24c] Actually, at high temperature, the increasing of gauche conformation will lead to the shortened length of alkyl chains of the amphiphiles, thereby the smaller layer spacing.[16,28] Further decreasing temperature leads to the formation of solid state, as proved by one peak at $2\theta \approx 20°$ (Figure 5c and inset). The solid structure is stable until the temperature falls down to 66 °C, where a solid-to-solid phase transition occurs. Hence, the mesophase sequence of PM-1/C_8BphC_{10}N during cooling run can be concluded to Iso−SmA−SmC−Solid2−Solid1. Very similar mesophase sequences are observed for other complexes, PM-1/

(25) (a) Takenaka, Y.; Osakada, K.; Nakano, M.; Ikeda, T. *Macromolecules* **2003**, *36*, 1414. (b) Dong, Y. P.; Lam, J. W. Y.; Peng, H.; Cheuk, K. K. L.; Kwok, H. S.; Tang, B. Z. *Macromolecules* **2004**, *37*, 6408. (c) Cui, L.; Zhao, Y. *Chem. Mater.* **2004**, *16*, 2076. (d) Kong, X.; Tang, B. Z. *Chem. Mater.* **1998**, *10*, 3352. (e) Sudhölter, E. J. R.; Engberts, J. B. F. N.; de Jeu, W. H. *J. Phys. Chem.* **1982**, *86*, 1908.
(26) Bu, W.; Wu, L.; Zhang, X.; Tang, A.-C. *J. Phys. Chem. B* **2003**, *107*, 13425.
(27) Rocchoccioli-Deltcheff, C.; Fournier, M.; Franck, R.; Thouvenot, R. *Inorg. Chem.* **1983**, *22*, 207.
(28) (a) Abdallah, D. J.; Robertson, A.; Hsu, H. F.; Weiss, R. G. *J. Am. Chem. Soc.* **2000**, *122*, 3053. (b) Kanazawa, A.; Ikeda, T. *Chem. Mater.* **2000**, *12*, 3776. (c) Traube, H.; Haynes, D. H. *Chem. Phys. Lipids* **1971**, *7*, 324.

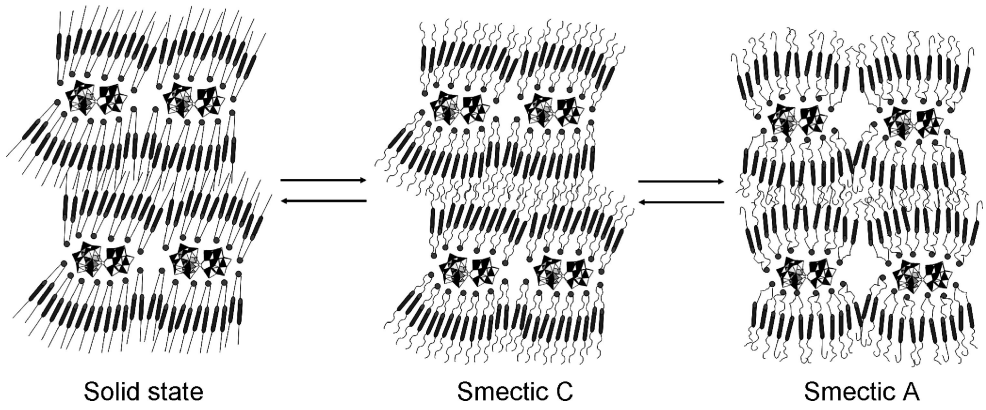

Figure 6. Schematic packing model and mesophases transition of PM-1/C_nBphC_{10}N during their heating and cooling process.

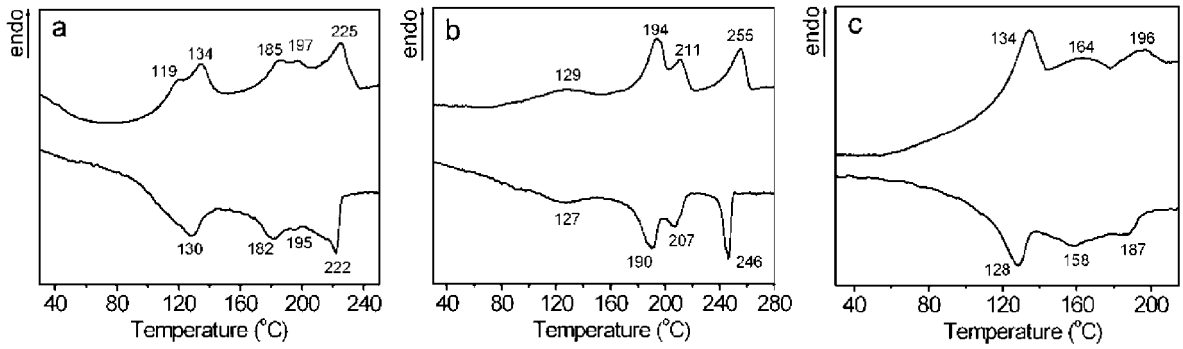

Figure 7. DSC curves of (a) PM-2/C_8BphC_{10}N, (b) PM-3/C_8BphC_{10}N, and (c) PM-4/C_8BphC_{10}N on their second heating and second cooling process.

C_nBphC_{10}N, and the layer spacing values are listed in Table S3. Combing the microscopic observations and the XRD patterns, we suggest a schematic packing model and structure change of PM-1/C_nBphC_{10}N with regard to the temperature, as shown in Figure 6.

The above data suggest that a variety of the tail length of the amphiphiles cannot cause change of mesophases of PM-1/C_nBphC_{10}N. It is interesting to speculate the reason that the mesophase type of amphiphiles depends on the tail length, whereas the same dependence is not observed in their corresponding complexes with PM-1. Comparing with C_nBphC_{10}N, PM-1/C_nBphC_{10}N exhibits lower melting temperature and higher clearing point. We have showed that the curvature of the elliptical cluster could induce the decrease of melting temperature, and strong electrostatic interaction between amphiphile and cluster plays an important role for the stabilization of smectic phase.[16] In fact, PMs are nanosized cluster possessing the similar size as that of cationic organic molecule, and it is reasonable to assume that the nature of PMs may affect the phase behavior of the complexes. Following this, we detect the influence of PMs on the LC behavior of complexes.

Influence of PMs on LC Behavior of Complexes. To understand the LC property dependence of the complexes on the component structure of PMs, we use a certain amphiphile C_8BphC_{10}N to encapsulate different PMs with various shape and surface charge density and investigate the influence of inorganic core on the mesophase of PM-m/C_8BphC_{10}N. Thus, we characterized a series of complexes, PM-2/C_8BphC_{10}N, PM-3/C_8BphC_{10}N, and PM-4/C_8BphC_{10}N, by DSC, POM, and XRD, respectively. From the DSC curves (Figure 7), we can clearly see the difference of transition temperature among these complexes as well as PM-1/C_8BphC_{10}N. The temperatures and enthalpies of mesophase transitions of these three complexes are also summarized in Table 1.

The mesophases of PM-2/C_8BphC_{10}N, PM-3/C_8BphC_{10}N, and PM-4/C_8BphC_{10}N were further investigated by POM. As seen in Figure 8, PM-2/C_8BphC_{10}N displays a smectic A phase at 218 °C. When the smectic A phase is continuously cooled, a small fan-shaped texture (Figure 8b) is observed at 194 °C. The fan texture changes quickly into broken fan texture (Figure 8c), suggesting a smectic C phase. For PM-3/C_8BphC_{10}N, lancet texture is observed at 240 °C (Figure 8d). The lancet texture is a common characteristic of smectic B phase, particularly for materials with a direct transition from the isotropic liquid.[29] On further cooling, a mosaic texture (Figure 8e) is observed at 206 °C, suggesting crystalline smectic phase. In the case of PM-4/C_8BphC_{10}N, smectic A (Figure 8f) and smectic C phases (Figure 8g) are observed.

We further examined XRD patterns of the complexes to identify the exact LC phases. The XRD pattern of PM-2/C_8BphC_{10}N at 208 °C (Figure 9a) shows a smectic A phase with layer spacing of 5.2 nm. When the temperature is decreased to 193 °C, three nonequidistant peaks are observed in the small-angle region. The diffraction peak positions just fit the ratio of $1:1/\sqrt{3}:1/2$, corresponding to the hexagonal columnar phase. However, the hexagonal phase is transient and quickly transforms into a smectic C phase with decreasing temperature. Normally, it is curious that the hexagonal

(29) Dierking, I. *Textures of Liquid Crystals*; Wiley-VCH: Weinheim, Germany, 2003; pp 135–139 and references therein.

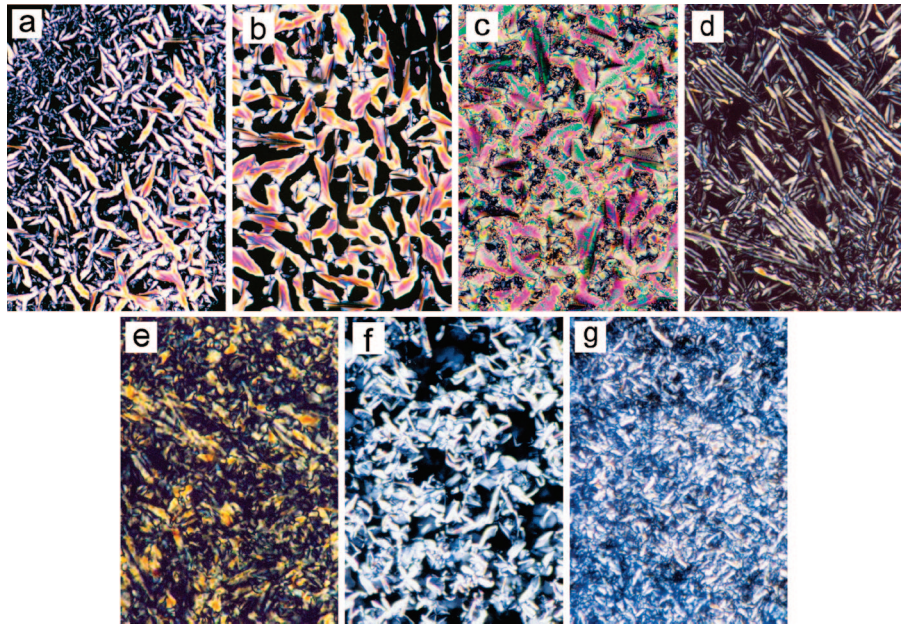

Figure 8. Polarizing optical micrographs of (a) PM-2/$C_8BphC_{10}N$ at 218 °C, (b) PM-2/$C_8BphC_{10}N$ at 194 °C, (c) PM-2/$C_8BphC_{10}N$ at 170 °C, (d) PM-3/$C_8BphC_{10}N$ at 240 °C, (e) PM-3/$C_8BphC_{10}N$ at 206 °C, (f) PM-4/$C_8BphC_{10}N$ at 188 °C, and (g) PM-4/$C_8BphC_{10}N$ at 152 °C (magnification: ×200) on cooling process.

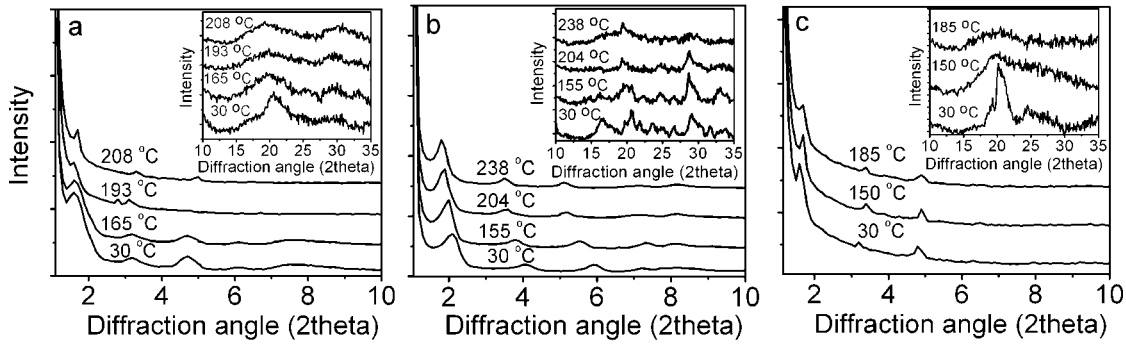

Figure 9. Variable-temperature X-ray diffraction patterns of (a) PM-2/$C_8BphC_{10}N$, (b) PM-3/$C_8BphC_{10}N$, and (c) PM-4/$C_8BphC_{10}N$ (inset: wide-angle X-ray diffraction).

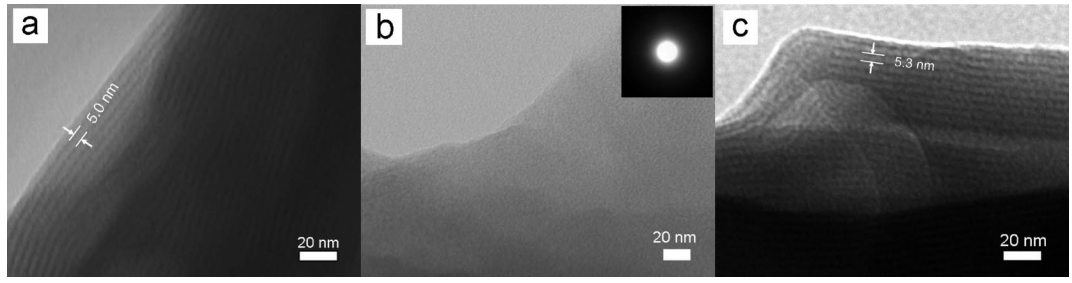

Figure 10. TEM image of PM-3/$C_8BphC_{10}N$ crystallized at different temperature from the isotropic melt and then gradually cooled to ambient temperature: (a) at 213 °C, (b) at 194 °C (inset shows the electron diffraction pattern), and (c) at 175 °C.

phase appears between smectic A and smectic C, and to our knowledge, there is no precedent for such a phase transition. In order to confirm the assignment of hexagonal structure, we tried to obtain more evidence from the measurement of TEM (Figure 10). Figure 10a shows the ordered lamellar morphology at 213 °C, and the lamellar structure gives 5.0 nm of layer-to-layer spacing, which is consistent with the result of XRD. The dark region corresponds to the inorganic PM-2 clusters whereas the light region corresponds to the organic amphiphiles. Figure 10b gives the morphology at 194 °C; PM-2 clusters appear as dark spots embedded in a bright matrix of amphiphile molecules. The related electron diffraction pattern (inset) reveals disordered morphology. Although the result of TEM cannot provide enough information to fit the XRD data, the results suggest that the transient mesophase is not a lamellar structure. Discreetly, we here do not give a clear verdict after several times of repeated measurement. When the temperature decreases to 175 °C, layered structure appear again as shown in Figure 10c, and the lamellar spacing is estimated as 5.3 nm. Thus, the temporary mesophase sequence of PM-2/$C_8BphC_{10}N$ can be concluded to a process of Iso−SmA−X−SmC−Solid2−Solid1. In the

case of PM-3/$C_8BphC_{10}N$, three equidistant diffraction peaks in the small-angle region accompanied by a strong peak at $2\theta \approx 20°$ are observed at 238 °C, as shown in Figure 9b. The presence of a single strong diffraction at $2\theta \approx 20°$ indicates a smectic B phase existing in its mesophase[30] because other higher order smectic phases show generally several sharp diffraction peaks in the wide angle region.[30a,31] On further cooling to 204 °C, a crystalline smectic phase (smectic X) is confirmed by several strong peaks in the wide-angle region. The XRD pattern of PM-4/$C_8BphC_{10}N$ at 185 °C (Figure 9c) can be identified as smectic A phase. When the temperature falls down to 150 °C, smectic C phase emerges. The above results clearly demonstrate that different mesophases in PM-containing LC materials can be generated by the suitable selection of PMs.

By comparing the thermal behaviors, we can observe that there are different transition temperature and LC sequence between PM-1/$C_8BphC_{10}N$ and PM-2/$C_8BphC_{10}N$. One possible explanation should be that the shape of PMs can cause changes of overall packing arrangement of the amphiphiles which electrostatically combine with them in the complexes. PM-1 is an elliptical cluster, and the amphiphile molecules to cover it could align along its long axis, which is favorable for the formation of lamellar structure.[12b,16] We have proposed that the aggregated manner of amphiphiles around the elliptical cluster is similar to that of the original amphiphile.[16b] In the case of spherical cluster PM-2, it is likely that large curvature be introduced into the complexes, which leads to the difference of aggregated manner comparing with the complex of PM-1. This comparison indicates that the shape of PMs can influence on the thermal properties of the complexes. In spite of the geometric resemblance between PM-2 and PM-3, PM-3/$C_8BphC_{10}N$ exhibit ordered smectic B phase. In fact, there is a general tendency that ordered smectic phase can form when the diameter of the inorganic cluster is comparable to the diameter of amphiphiles. In the Experimental Section, we have concluded that the sizes of PM-2 and PM-3 are the same, whereas the surface charge density of PM-3 is lower than that of PM-2. The low surface charge density of PM-3 results in the number of amphiphile molecules in PM-3/$C_8BphC_{10}N$ is less than that of PM-2/$C_8BphC_{10}N$. We, therefore, suggest that the diameter of PM-3 is comparable to the cross-section area of amphiphiles, and this allows PM-3/$C_8BphC_{10}N$ to possess ordered smectic B phase. Liquidlike amphiphile molecules in the complex PM-2/$C_8BphC_{10}N$ occupy larger cross-section area and molecular volume in mesophase than that of PM-3, thus leading to disordered smectic phases. Comparing with PM-3/$C_8BphC_{10}N$, although the number of amphiphiles in PM-4/$C_8BphC_{10}N$ is identical, the planar PM-4 does not lead to ordered smectic phase like PM-3. This is also result from the difference of shape between PM-3 and PM-4 (see Figure 1).

We suppose, therefore, that the segregation of PMs and amphiphiles as well as packing arrangement of the complexes is determined by several factors, including hydrophobic and electrostatic interaction, overall molecular shape, the number of amphiphile molecules in a complex, and the surface charge density of PMs. The variety of these factors induces the complexes to exhibit different phase transition temperatures and mesophase architectures.

Conclusion

The cationic amphiphiles, dialkyldimethylammonium bromides inserted biphenyl group in each of the alkyl chains, and their corresponding amphiphile-encapsulated polyoxometalate complexes have been prepared. All the amphiphiles and complexes exhibit typical thermotropic LC characters. The mesophase type of amphiphiles $C_nBphC_{10}N$ is dependent on the variety of tail length; however, the relationship between the tail length and the mesophase type is not observed in the complex PM-1/$C_nBphC_{10}N$. All the complexes PM-1/$C_nBphC_{10}N$ form smectic A and smectic C phase with tail chains interdigitated partially. A structural model for the molecular organization of PM-1/$C_nBphC_{10}N$ was proposed. It was found that the balance among alkyl chain volume, shape, and surface charge density of PMs plays an important role in the formation of the phase architectures. Different LC phases, such as smectic B and crystalline smectic phases, were observed by changing the shape and surface charge density of PMs from elliptical cluster PM-1 to spherical clusters PM-2 and PM-3 and further to planar cluster PM-4 in the complexes of PM-m/$C_8BphC_{10}N$. The present results show that phase behaviors of this kind of building block can be adjusted through the choice of inorganic cluster PMs. We believe that this research will be helpful for the design, facile tuning, and production of PMs-containing liquid crystals.

Acknowledgment. We acknowledge the financial support from National Basic Research Program (2007CB808003), National Natural Science Foundation of China (20473032, 20731160002), PCSIRT of Ministry of Education of China (IRT0422), 111 Project (B06009), and Open Project of State Key Laboratory of Polymer Physics and Chemistry of CAS.

Supporting Information Available: Phase transition temperatures, enthalpies, and polarizing optical images of amphiphiles and complexes. This material is available free of charge via the Internet at http://pubs.acs.org.

CM702955J

(30) (a) Xu, J. W.; Toh, C. L.; Liu, X. M.; Wang, S. F.; He, C. B.; Lu, X. H. *Macromolecules* **2005**, *38*, 1684. (b) Hsu, C.-S.; Lin, J.-H.; Chou, L.-R.; Hsiue, G.-H. *Macromolecules* **1992**, *25*, 7126. (c) de Vries, A. *Chem. Phys. Lett.* **1974**, *28*, 252.

(31) (a) Kelker, H.; Hatz, R. *Handbook of Liquid Crystals*; Verlag Chemie GmbH: Weinheim, Germany, 1980; pp 231–242. (b) Krigbaum, W. R. J.; Watanabe, J.; Ishikawa, T. *Macromolecules* **1983**, *16*, 1271.